Research Article Vol. 2, No. 7 / July 2015 / Optica 616

Epsilon-near-zero Al-doped ZnO for ultrafast switching at telecom wavelengths

N. Kinsey,[1] C. DeVault,[2] J. Kim,[1] M. Ferrera,[1,3] V. M. Shalaev,[1] and A. Boltasseva[1,*]

[1]School of Electrical and Computer Engineering and Birck Nanotechnology Center, Purdue University, West Lafayette, Indiana 47907, USA
[2]Department of Physics and Birck Nanotechnology Center, Purdue University, West Lafayette, Indiana 47907, USA
[3]School of Engineering and Physical Sciences, Heriot-Watt University, Edinburgh, Scotland EH14 4AS, UK
*Corresponding author: aeb@purdue.edu

Received 20 March 2015; revised 19 May 2015; accepted 1 June 2015 (Doc. ID 236529); published 2 July 2015

Transparent conducting oxides have recently gained great attention as CMOS-compatible materials for applications in nanophotonics due to their low optical loss, metal-like behavior, versatile/tailorable optical properties, and established fabrication procedures. In particular, aluminum-doped zinc oxide (AZO) is very attractive because its dielectric permittivity can be engineered over a broad range in the near-IR and IR. However, despite all these beneficial features, the slow (>100 ps) electron-hole recombination time typical of these compounds still represents a fundamental limitation impeding ultrafast optical modulation. Here we report the first epsilon-near-zero AZO thin films that simultaneously exhibit ultrafast carrier dynamics (excitation and recombination time below 1 ps) and an outstanding reflectance modulation up to 40% for very low pump fluence levels (<4 mJ/cm^2) at a telecom wavelength of 1.3 μm. The unique properties of the demonstrated AZO thin films are the result of a low-temperature fabrication procedure promoting deep-level defects within the film and an ultrahigh carrier concentration.

OCIS codes: (160.4670) Optical materials; (300.6530) Spectroscopy, ultrafast; (230.1150) All-optical devices; (240.6380) Spectroscopy, modulation.

http://dx.doi.org/10.1364/OPTICA.2.000616

1. INTRODUCTION

A. TCO-Based Tunable Nanophotonics

With the advent of plasmonics and metamaterials, it has become of paramount importance to develop new CMOS-compatible platforms possessing metal-like behavior and great optical transparency. Transparent conducting oxides (TCOs) are a class of materials that are well known for their optical transparency combined with a high electrical conductivity, and consequently, they appear to be critical for enabling novel tunable nanophotonic devices. TCOs such as indium-doped tin oxide (ITO) and indium + gallium-doped zinc oxide have been widely used in industrial applications for touchscreen displays, transparent electrodes on solar panels, and more recently in televisions [1,2]. As a result of their widespread industrial use, CMOS-compatible deposition techniques have been demonstrated that enable the growth of high-quality room-temperature thin films [3–9].

One of the valuable assets of TCOs is the intrinsic tunability of the optical properties. Since TCOs can sustain extremely heavy doping without consistent degeneration of their morphological structure, very high carrier concentrations (~10^{20} cm^{-3}) can be achieved [10–14]. Subsequently, the optical properties of these materials can be tailored in many ways such as by altering the deposition conditions through postprocessing steps (e.g., annealing) and/or by varying the material stoichiometry [11,13,15–19]. This enables one material to serve several roles. For instance, a lowly doped TCO can be used as a dielectric material in the near-infrared (NIR) range with an index near 2, while a highly doped TCO can serve as a metal to support surface plasmon oscillations [20,21].

Additionally, TCOs exhibit the potential for both electrical and optical excitation, allowing a dynamic modification of their optical properties [14,22–25]. The application of an electric field results in carrier accumulation or depletion, causing a temporary change in the optical properties within a thin layer (~2–5 nm) [26]. Even though this method can have extremely low energy dissipation in the femtojoule/bit range [27], the overall effect is generally limited by the *RC* delay of the specific electrical system to the gigahertz range in practice, although theoretically faster speeds could be attained.

Optical excitation of TCOs is also a potential method for dynamically tuning the optical properties of the films, similar to the approach demonstrated with other materials such as semiconductors and, recently, ITO nanorods [24,28,29]. In this approach, light with energy greater than the bandgap is used to excite valence band electrons into the conduction band, which in turn alters the properties of the material until they recombine and the material returns to equilibrium. This method has the benefit of generating free carriers throughout the bulk of the entire film (roughly hundres of nanometers thick) instead of only a few nanometers and, in principle, is only limited by the material

absorption time (~10 fs) and recombination time. In particular, a slow electron-hole recombination time is a fundamental burden for the realization of numerous all-optical devices. Consequently, our study is directly focused on solving this issue as well as increasing the limited available information about the optoelectric dynamics of TCOs.

B. Ultrafast Carrier Dynamics in Semiconductors

Carrier recombination in semiconductors (Si, GaAs, etc.) is governed by a plethora of processes including interband transitions, intraband relaxation, processes related to trap/defect/surface states (described by Shockley–Read–Hall mechanisms), and nonradiative (Auger) processes [30]. Generally, in bulk semiconductors, the interband recombination time is on the order of hundreds of picoseconds to nanoseconds [28,31], which limits the speed that all-optical devices relying on carrier generation–recombination can offer. Several techniques can be used to drastically decrease the recombination time, such as surface recombination, nanoparticle trapping, nonradiative recombination, and defect recombination centers [32–34]. For highly confined devices such as quantum wells or quantum dots, interband and intersubband recombination can also result in extremely fast recombination times on the order of 150 fs to a few picoseconds [35–37].

An example of such methodologies is low-temperature (<400°C) grown GaAs, where various defects are introduced into the crystal structure. The presence of defects drastically decreases the recombination time due to the introduction of midgap states according to $\tau = \frac{1}{N_t \sigma v_{\text{th}}}$, where N_t is the trap density, σ is the capture cross section, and v_{th} is the thermal velocity of carriers [30]. Recombination times on the order of 2 ps have routinely been achieved with such materials [33,34,38]. We note that additional methods of introducing defects are possible and are not specifically linked to low-temperature processing, such as doping to introduce deep-level defects ($\tau \sim 50$–100 ps) [39], ion bombardment ($\tau \sim 0.6$–4 ps) [40,41], and using amorphous/polycrystalline materials ($\tau \sim 0.8$–20 ps) [42]. However, these methods can result in the deterioration of fundamental optical (e.g., higher losses) and/or electronic (e.g., lower carrier mobility) properties, which may not be desirable for all applications [34].

Another example of reducing the recombination time is through Auger processes [30], which occur in semiconductors under extreme carrier concentrations of $\sim 10^{19}$ cm^{-3} and larger (for silicon). Recombination times as small as 100 fs have been achieved in silicon for a carrier density of 10^{21} cm^{-3}, although the recombination time will vary with the induced excess carriers (i.e., pump fluence) and the nonradiative nature of the effects can lead to a significant thermal buildup, potentially limiting the speed of the device [43].

C. Optical Switching at Epsilon-Near-Zero

In addition to an ultrafast temporal response, it is also beneficial to have a large change in the optical properties of the dynamic material. To enhance the amplitude of the material response, we propose operating in the epsilon-near-zero (ENZ) regime [25,44–46]. As shown in Fig. 1, operating in the ENZ regime (i.e., $n < 1$) produces larger absolute changes in the reflection for a fixed change in the refractive index ($\Delta n = -0.1$ in a purely real medium). This can be understood by considering the change in magnitude with respect to the initial index, e.g., a change of −0.1 for an initial index of 0.2 is 50%, whereas for an initial index of 2, it is only a 5% change. Consequently, this makes the ENZ regime an attractive region for maximizing the performance of dynamic devices.

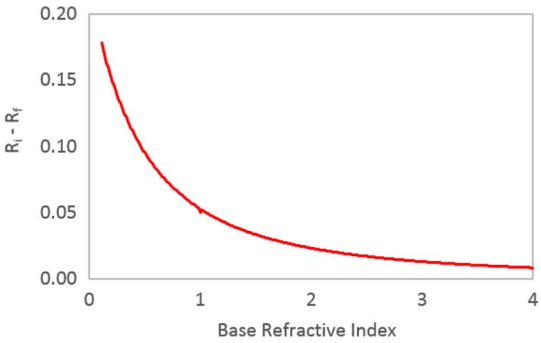

Fig. 1. Absolute change in the reflection of a purely real (i.e., $\text{Im}\{n\} = 0$) material versus base refractive index provided an index change of $\Delta n = -0.1$. The magnitude of reflection is calculated using the Fresnel equations at a single interface between air ($n_o = 1$) and the material assuming normal incidence. Note that operating in the epsilon-near-zero regime (i.e., $n < 1$) provides larger absolute changes in the reflection for the same change in the refractive index.

Traditional semiconductors cannot achieve ENZ operation at the technologically important telecommunication wavelengths due to their large background permittivity and low dopant solubility—even other TCOs struggle with this problem [47]. While some TCOs can achieve ENZ properties at telecom, all currently published works have yet to demonstrate both a large optical response and a short recombination time.

In this work, we develop a CMOS-compatible, oxygen-deprived aluminum-doped zinc oxide (AZO) film that achieves both of the desired properties simultaneously. Our unique material recovers in less than 1 ps with relative variations of the transient reflectivity ($\Delta R/Ro$) and transmissivity ($\Delta T/To$) as large as 40% and 30%, respectively. Both the ultrafast recombination and the extremely high intrinsic carrier concentration ($\sim 10^{21}$ cm^{-3}) are a direct consequence of our unique low-temperature fabrication process, which induces deep-level defects to produce the required number of donor centers (see Section 2 and Supplement 1).

Consequently, our AZO thin films satisfy several key attributes of dynamic materials simultaneously: (1) large intrinsic carrier concentration to enable ENZ properties at the technologically important telecommunication wavelengths (which enhances the optical/electrical tunability), (2) low-temperature deposition, which does not impede conductivity and transparency, (3) maturity of the fabrication and nanopatterning process, (4) CMOS compatibility, and (5) ultrafast electron-hole recombination dynamics. In order to further investigate the applicability of our oxygen-deprived AZO, we also propose a scheme for an all-optical plasmonic modulator using CMOS-compatible materials that achieves 3 dB signal attenuation in 7.5 μm with less than 0.1 dB/μm insertion loss (see Supplement 1).

2. RESULTS

A. Oxygen-Deprived AZO Thin Films

A 350 nm thick AZO film (hereto referred to as-grown AZO) was deposited at room temperature on a fused silica substrate by pulsed laser ablation of a 2 wt. % AZO target [48,49]. Additionally, our AZO films are deposited under low oxygen

partial pressure to induce oxygen vacancies (for more information, see Supplement 1) [16]. These oxygen vacancies push the already high carrier concentration provided by the doping process even further, giving rise to an extremely high intrinsic carrier concentration within the material that can be controlled by varying the oxygen pressure during deposition, or through annealing in an oxygen-rich environment [15]. Although pulsed laser ablation is not a CMOS-compatible deposition technique, other AZO and ZnO films have been reported using fully CMOS-compatible techniques such as atomic layer deposition, such that our films could be made fully CMOS-compatible [7,8].

To dynamically modify the carrier concentration within the film, the material is pumped by light with photon energy greater than the bandgap (~3.5 eV). The excess free electrons then cause a change in the optical properties (reflection, transmission, and absorption) of the probe through the Drude dispersion, which is added to the background or intrinsic permittivity of the material. Then, the system recovers through the recombination of excess carriers, returning to its original state.

B. Preliminary Material Characterization

To determine the proper pump and probe wavelengths, the linear optical properties of the as-grown AZO film are required (see Fig. 2). The permittivity of the sample was extracted from spectroscopic ellipsometry using a Drude–Lorentz model (see Supplement 1) that describes the intrinsic material response. Consequently, the ENZ regime of the material (1.1–1.5 μm) is extracted and shaded red in Fig. 2(a). Additionally, the linear transmission spectrum of the sample is shown in Fig. 2(b), which illustrates the band edge of the material. As can be seen from both curves, the band edge of the as-grown AZO film lies at ~350 nm (shaded green). Consequently, light shorter than 350 nm must be used to pump the AZO. Therefore, a combination of 1.3 μm and 325 nm was chosen, as it provides a pump greater than the bandgap energy and a probe at a technologically relevant wavelength that is also near the ENZ point of the material [see Fig. 2(a)]. While more efficient absorption of the pump could be achieved with slightly shorter wavelengths, it is beneficial to keep the pump wavelength at as low an energy as possible to aid the efficiency of conversion as well as to minimize losses in optics such as lenses and mirrors.

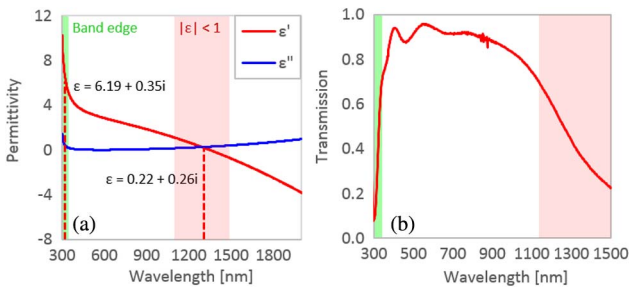

Fig. 2. (a) Complex permittivity of the 350 nm as-grown AZO film as extracted from spectroscopic ellipsometry. The green shaded area represents wavelengths above the band edge of the AZO, and the red shaded area represents the ENZ regime, i.e., $|n| < 1$. The permittivities of the AZO at the two test wavelengths are given for reference. (b) Transmission spectrum of the 350 nm AZO film obtained using a spectrophotometer.

C. Optical Setup

An illustration of the pump–probe system used to test the as-grown AZO films is depicted in Fig. 3(a). Collinear 1.3 μm and 650 nm light is brought into the system from the bottom right and separated by a dichroic filter (F1). 650 nm is focused onto a BBO crystal to generate the second harmonic, and filtered to remove any residual 650 nm. 1.3 μm is filtered by a long-pass filter (F3) to remove any 650 nm light and directed through a computer-controlled retroreflector, providing a delay line. Both 1.3 μm and 650 nm beams are focused onto the sample, where the 1.3 μm is filtered and collected by an InGaAs detector (D1). A more detailed description of the experimental methods is found in Supplement 1.

D. Transient Reflectivity and Transmissivity

The normalized reflection and transmission as a function of the pump–probe pulse delay are shown in Figs. 3(b) and 3(c), respectively, for the 350 nm as-grown AZO thin film under several incident pump fluence levels. Upon closer examination of these results, a few important points arise: (1) the transient effect is fully recovered (from start to finish) within 1 ps (greater than 1 THz potential modulation speed) with a relaxation time of less than 500 fs; (2) the change in the transmission/reflection is relatively large, with all measurements having at least a 10% variation and a peak change of 40% for a base reflection at the probe wavelength of 25% and transmission of 40%; (3) the UV fluence used is at least an order of magnitude below the typical damage threshold for dielectrics (~100 mJ/cm^2 for femtosecond pulses [50]), indicating that the effect could be further increased; (4) a total pulse energy of only a few microjoules is required to induce the effects

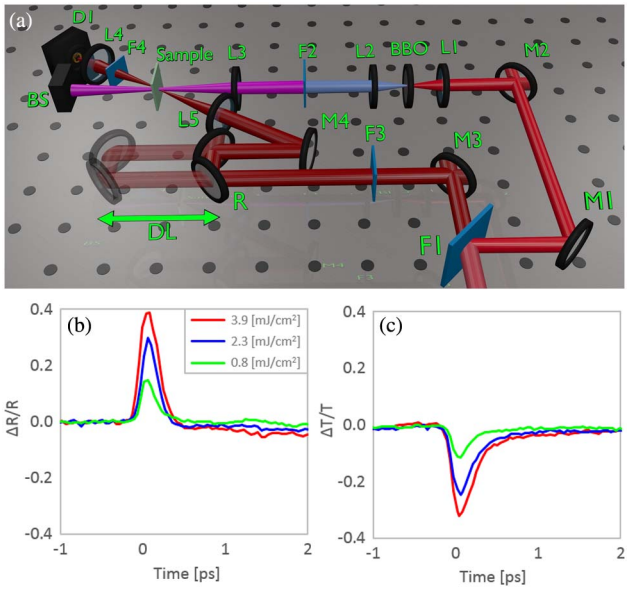

Fig. 3. (a) Schematic of the pump-probe setup. Filter F1 transmits 1.3 μm and reflects 650 nm light. F3 removes residual 650 nm. *R* provides a delay line. Lenses L1 and L2 focus the light onto BBO to generate 325 nm light. Filter F2 removes residual 650 nm. Lenses L3 and L5 focus light onto the sample. F4 filters any stray light for detector D1. Normalized change in the (b) reflected power and (c) transmitted power as a function of the delay time between the pump and probe pulses. The absolute reflection (transmission) of the AZO sample without pumping is 25% (40%) at 1.3 μm.

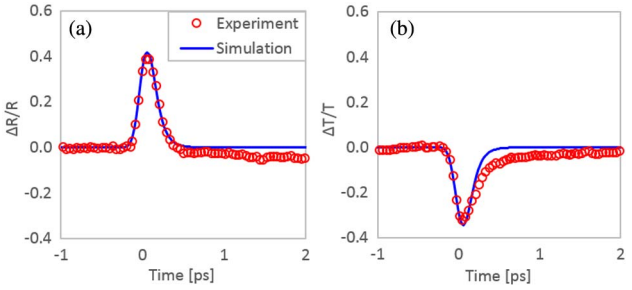

Fig. 4. Fitted change in (a) reflection and (b) transmission for the 350 nm thick as-grown AZO film under a fluence of 3.9 mJ/cm^2.

shown here; (5) the material thickness is compatible with current integrated technologies, which is especially critical, since the material properties (e.g., carrier concentration) may differ drastically in thin films when compared to bulk films.

One of the key parameters for dynamic materials is the maximum achievable change in the optical properties, which in this case is the result of excess carrier generation. Thus, it is critical to understand the carrier concentration that was achieved during the experiment. To extract this value, a theoretical model has been used, which is then fitted with the experimental results where the transfer matrix approach was used to determine the linear reflection and transmission of the thin film sample for both the pumped and unpumped cases (see Supplement 1). In Fig. 4 the results of the fitting are shown, where excellent agreement is found between calculation and experiment. However, there is a slight discrepancy in the transmission measurement toward the end of the decay (a small offset, ~3%) in both the reflection and transmission (i.e., they do not return to zero). This small offset is believed to be the result of lattice heating from excited electrons relaxing to the band edge, which plays a role on significantly longer time scales (hundreds of picoseconds to nanoseconds) [51]. This minimal alteration of the optical properties is not permanent (e.g., material damage), and the AZO returns to equilibrium within 1 ms (repetition rate of the laser source). In addition, these effects have very little influence on the ultrashort response of the as-grown AZO and therefore do not significantly influence our extraction of the excess carrier concentration or decay time in the sample. Additionally, such offsets were not present in all films tested, suggesting the ability to engineer or remove the effect. However, for devices, this small dissipation of thermal energy may lead to unwanted collective thermal effects such as a modification of the refractive index, thereby limiting the maximum achievable duty cycle in the device. Despite this, general trends can be highlighted. Most solid materials have a thermal change in the refractive index on the order of $dn/dT \sim 10^{-5}$ K^{-1} [51] (used in the absence of data for ZnO and AZO). If we assume even a radical steady-state temperature of 600°C for a high-speed AZO-based device, we can expect a change in the base refractive index of $\Delta n \sim 0.006$, still two orders of magnitude below the changes in refractive index induced by the control pulses (see Table 1). The contribution of this, or more complex effects, to the overall response of a specific device is suggested as an area for future studies.

With a successful fitting achieved, the carrier distribution can be obtained. From the model, an average excess carrier density of 0.7×10^{20} cm^{-3} is estimated within the sample's thickness of 350 nm at the focus of the pump, corresponding to a peak of 1.4×10^{20} cm^{-3} near the surface at time $t = 0$, which is similar to the values reported for optically modified ITO nanorods [24]. For electrical tuning, a peak $\delta N = 6.7 \times 10^{20}$ cm^{-3} has been achieved, although it is important to remember that these densities are achieved only within a few nanometers of the surface and not throughout the bulk of the material [26]. In fact, considering an accumulated layer thickness of 5 nm for the δN listed above, the raw number of carriers induced using optical excitation is 10× more than what was reportedly achieved through electrical biasing.

The excess carrier density and recombination time have been extracted for the listed fluences and are presented in Table 1 together with the maximum relative changes in reflectivity and transmissivity, intrinsic carrier concentration, electron-hole recombination time, and the variation in the complex refractive index. Here, we see that the range of average carrier densities induced in the sample is on the order of 10^{19} cm^{-3} (roughly 5%–10% of the intrinsic concentration), being measured for an incident energy of a few microjoules. This is also particularly interesting considering the large change in the optical properties that is observed, likely arising from operating in the ENZ regime.

3. DISCUSSION

It is important to mention that the carrier densities reported in Table 1 underestimate the actual carrier density achieved within the material after pumping due to the temporal resolution limit of the system. Although the actual induced carrier density is larger, we report in Table 1 a conservative estimate of the achieved carrier density at the pump focus averaged over the thickness of the material as extracted from the experiment using two spatially finite width pulses.

The ultrafast temporal response is believed to be the result of defect-enhanced (Shockley–Read–Hall) recombination that arises due to the way the AZO is grown [30]. By depositing the AZO with our unique technique, a large density of deep-level defects are created in the film [52,53]. These deep-level defects dramatically reduce the recombination time for electrons. As was discussed previously, similar situations have been investigated in low-temperature deposited gallium arsenide (LT-GaAs), as well

Table 1. Summary of the Extracted Properties of the 350 nm As-Grown AZO Sample Including the Intrinsic Concentration[a]

Pump Fluence [mJ/cm^2]	Max. ΔR [%]	Max. ΔT [%]	Intrinsic Concentration [cm^{-3}]	Rec. Time [fs]	Avg. Induced Carriers [cm^{-3}]	AZO $\Delta n + i\Delta k$
1.0	15	−12	9.8×10^{20}	100	0.2×10^{20}	$-0.07 + i0.07$
2.4	30	−25	9.8×10^{20}	92	0.5×10^{20}	$-0.14 + i0.16$
3.6	39	−32	9.8×10^{20}	88	0.7×10^{20}	$-0.17 + i0.25$

[a]The max. ΔR and ΔT values are the peak relative changes in reflection and transmission, respectively, and $\Delta n + \Delta k$ correspond to the maximum changes induced in the material properties.

as in several other specially grown materials, where the time scale of the process is attributed to defect-enhanced recombination [32,34]. However, one key distinction of the as-grown AZO from other materials is the magnitude of the effect. Generally for LT-GaAs and other semiconductors, the measured change in reflectivity is ~2%, although various pulse energies and wavelengths are used in the literature, which makes a direct comparison of the amplitude difficult. However, our as-grown AZO is shown to achieve speeds that are generally 2–3 × faster than those reported for LT-GaAs [34]. Electrical tuning methods in silicon, which make use of carrier accumulation/depletion, rely on diffusion to remove carriers and can be faster. However, these devices are well known to be limited by the capacitor charging time (*RC* delay) to a few tens of gigahertz and recently up to 100 GHz [54]—at best an order of magnitude slower than the as-grown AZO [55–57]. As for recent works optically tuning ITO nanorods, we note at most an effect 2× larger and 6× faster for lower pump fluence levels than was previously reported, without the need for complicated nanorod structures [24].

Furthermore, the fact that the total carrier density is not radically changing to produce the modulation effect results in recombination times that are relatively constant. This can be an important feature for practical devices such that the temporal response of the system does not change based on pump fluence (as it would with other effects such as Auger recombination), enabling the use of the minimal energy without sacrificing speed, or for more specific applications such as high-speed analog encoding and data processing. As a demonstration of such a device, an all-optical hybrid plasmonic modulator has been designed using a suite of CMOS-compatible materials (see Supplement 1). The device is shown to exhibit a 0.4 dB/μm modulation depth (0.2 dB/μm extinction ratio) with coupling losses less than 0.1 dB/μm, competitive with other all-optical plasmonic modulators in the literature.

In addition, there is the potential for an inverted modulator by properly controlling the initial permittivity of the as-grown AZO film. Here, the base permittivity of the film is already near zero (i.e., less than unity), such that inducing additional free electrons causes the material to appear "more metallic," thereby increasing the reflection. However, if the as-grown AZO film was grown with a lower intrinsic carrier concentration such that the material's permittivity was greater than unity at 1.3 μm, adding additional carriers would cause a decrease in the reflection. This flexibility enables the potential for both positive and negative logic devices from the same material by simply altering the deposition conditions.

Finally, the ultrafast response of the as-grown AZO opens many additional applications beyond high-speed data processing. One application could be in the area of terahertz wave generation—consistently a challenge for the field. By pumping the as-grown AZO with an ultrafast 325 nm pulse, a terahertz modulation of the conductivity is achieved that, when combined with the proper electrical circuitry, can serve as a terahertz radiation source. The quick response is also valuable for measuring the temporal shape of short optical pulses, which can be quite difficult in the UV range due to the inefficiency of traditional materials such as silicon and GaAs, assuming they were configured to detect ultrafast signals. Combining an as-grown AZO-based detector with built-in electrical delays and phase-locking electronics, an integrated optoelectric sampling detector can be realized that is capable of a few picosecond resolution. This technique could be much more compact and simple to use than traditional autocorrelators requiring two optical beams.

4. CONCLUSION

The ability to achieve large modulation without sacrificing speed is critical for future photonic and hybrid photonic–electronic devices. TCOs, and AZO in particular, are very promising materials for realizing high-performance dynamic devices and can be modified either with the application of an electric field or through optical excitation. Although both techniques are favorable methods for realizing dynamic devices, all-optical methods are beneficial due to high operating speeds and the lack of *RC* delay limits. Here, a unique fabrication strategy is introduced to optimize the photodynamic properties of AZO thin films while achieving ENZ properties at telecommunication wavelengths. Both the reflectivity and transmissivity were investigated using ultrafast pump–probe spectroscopy, whereby a large ($\Delta R/R_0 = 40\%$ with $\Delta T/T_0 = 30\%$) and ultrafast (<1 ps) response in both transmission and reflection was observed for all applied fluences. By modeling the physics behind the carrier dynamics, the excess carrier density within the material was extracted along with the recombination time of the process, which is believed to be the result of defect-enhanced recombination, enabling verified speeds exceeding 1 THz. With only a few microjoules of applied energy, the average carrier concentration within the bulk of the material (~350 nm) was changed by roughly 10%, resulting in a raw modification of the carrier density that is 10× larger than reported electrical biasing of TCOs. Providing a more uniform distribution of carriers within the bulk of a material without sacrificing speed is beneficial for a wide range of applications such as optical modulators and tunable metasurfaces to more efficiently utilize the entire available dynamic material. Consequently, AZO is shown to be a unique, promising, and CMOS-compatible material for all-optical dynamic devices in the near future.

Funding. Air Force Office of Scientific Research (AFOSR) (FA9550-14-1-0138); Marie Curie Outgoing International Fellowship (329346); National Science Foundation (NSF) (DMR1120923); Office of Naval Research (ONR) (N00014-10-1-0942).

Acknowledgment. We thank Dr. Urcan Guler and Amr Shaltout for useful discussions during this work.

See Supplement 1 for supporting content.

REFERENCES

1. K. Nomura, H. Ohta, A. Takagi, T. Kamiya, M. Hirano, and H. Hosono, "Room-temperature fabrication of transparent flexible thin-film transistors using amorphous oxide semiconductors," Nature **432**, 488–492 (2004).
2. H. Schmidt, H. Flugge, T. Winkler, T. Bulow, T. Riedl, and W. Kowalsky, "Efficient semitransparent inverted organic solar cells with indium tin oxide top electrode," Appl. Phys. Lett. **94**, 243302 (2009).
3. D. H. Levy, A. C. Scuderi, and L. M. Irving, "Methods of making thin film transistors comprising zinc-oxide-based semiconductor materials and transistors made thereby," U.S. patent 7,691,666 B2 (Apr. 6, 2010), Eastman Kodak Company.
4. Y. Li and B. S. Ong, "Thin film transistor using an oriented zinc oxide layer," European patent EP 1921681 A2 (May 14, 2008), Xerox Corporation.

5. M. Pinarbasi and J. Freitag, "Method of forming transparent zinc oxide layers for high efficiency photovoltaic cells," U.S. patent application 2011/0108099 A1 (11 November 2009), Solopower, Inc.
6. T. C. Gorjanc, D. Leong, C. Py, and D. Roth, "Room temperature deposition of ITO using r.f. magnetron sputtering," Thin Solid Films **413**, 181–185 (2002).
7. A. Frolich and M. Wegener, "Spectroscopic characterization of highly doped ZnO films grown by atomic-layer deposition for three-dimensional infrared metamaterials," Opt. Mater. Express **1**, 883–889 (2011).
8. A. K. Pradhan, R. M. Mundle, K. Santiago, J. R. Skuza, B. Xiao, K. D. Song, M. Bahoura, R. Cheaito, and P. E. Hopkins, "Extreme tunability in aluminum doped zinc oxide plasmonic materials for near-infrared applications," Sci. Rep. **4**, 6415 (2014).
9. D. N. Pier, C. F. Gay, R. D. Wieting, and H. J. Langeberg, "Solar cells incorporating transparent electrodes comprising hazy zinc oxide," U.S. patent 5,078,803 A (7 January 1992), Siemens Solar Industries L.P.
10. S. H. Brewer and S. Franzen, "Indium tin oxide plasma frequency dependence on sheet resistance and surface adlayers determined by reflectance FTIR spectroscopy," J. Phys. Chem. B **106**, 12986–12992 (2002).
11. S. Q. Li, P. Guo, L. Zhang, W. Zhou, T. W. Odom, T. Seideman, J. B. Ketterson, and R. P. H. Chang, "Infrared plasmonics with indium-tin-oxide nanorod arrays," ACS Nano **5**, 9161–9170 (2011).
12. E. Feigenbaum, K. Diest, and H. A. Atwater, "Unity-order index change in transparent conducting oxides at visible frequencies," Nano Lett. **10**, 2111–2116 (2010).
13. M. A. Noginov, L. Gu, J. Livenere, G. Zhu, A. K. Pradhan, R. Mundle, M. Bahoura, Y. A. Barnakov, and V. A. Podolskiy, "Transparent conductive oxides: plasmonic materials for telecom wavelengths," Appl. Phys. Lett. **99**, 021101 (2011).
14. M. Abb, B. Sepulveda, H. M. H. Chong, and O. L. Muskens, "Transparent conducting oxides for active hybrid metamaterial devices," J. Opt. **14**, 114007 (2012).
15. J. Kim, G. Naik, N. Emani, U. Guler, and A. Boltasseva, "Plasmonic resonances in nanostructured transparent conducting oxide films," IEEE J. Sel. Top. Quantum Electron. **19**, 1 (2013).
16. G. Naik, J. Kim, and A. Boltasseva, "Oxides and nitrides as alternative plasmonic materials in the optical range," Opt. Mater. Express **1**, 1090–1099 (2011).
17. T. R. Gordon, T. Paik, D. R. Klein, G. V. Naik, H. Caglayan, A. Boltasseva, and C. B. Murray, "Shape-dependent plasmonic response and directed self-assembly in a new semiconductor building block, indium-doped cadmium oxide (ICO)," Nano Lett. **13**, 2857–2863 (2013).
18. M. Kanehara, H. Koike, T. Yoshinaga, and T. Teranishi, "Indium tin oxide nanoparticles with compositionally tunable surface plasmon resonance frequencies in the near-IR region," J. Am. Chem. Soc. **131**, 17736–17737 (2009).
19. G. Garcia, R. Buonsanti, E. L. Runnerstrom, R. J. Mendelsberg, A. Llordes, A. Anders, T. J. Richardson, and D. J. Milliron, "Dynamically modulating the surface plasmon resonance of doped semiconductor nanocrystals," Nano Lett. **11**, 4415–4420 (2011).
20. G. V. Naik, V. M. Shalaev, and A. Boltasseva, "Alternative plasmonic materials: beyond gold and silver," Adv. Mater. **25**, 3264–3294 (2013).
21. C. Rhodes, S. Franzen, J.-P. Maria, M. Losego, D. N. Leonard, B. Laughlin, G. Duscher, and S. Weibel, "Surface plasmon resonance in conducting metal oxides," J. Opt. A Pure Appl. Opt. **100**, 054905 (2006).
22. H. Chen, R. J. Lamond, S. K. Pickus, L. Zhuo Ran, and V. J. Sorger, "A sub-lambda-size modulator beyond the efficiency-loss limit," IEEE Photon. J. **5**, 2202411 (2013).
23. V. Babicheva, N. Kinsey, G. V. Naik, M. Ferrera, A. V. Lavrinenko, V. M. Shalaev, and A. Boltasseva, "Towards CMOS-compatible nanophotonics: ultra-compact modulators using alternative plasmonic materials," Opt. Express **21**, 27326–27337 (2013).
24. D. B. Tice, S. Q. Li, M. Tagliazucchi, D. B. Buchholz, E. A. Weiss, and R. P. H. Chang, "Ultrafast modulation of the plasma frequency of vertically aligned indium tin oxide rods," Nano Lett. **14**, 1120–1126 (2014).
25. M. Abb, P. Albella, J. Aizpurua, and O. L. Muskens, "All-optical control of a single plasmonic nanoantenna-ITO hybrid," Nano Lett. **11**, 2457–2463 (2011).
26. V. J. Sorger, N. D. Lanzillotti-Kimura, R. Ma, and X. Zhang, "Ultra-compact silicon nanophotonic modulator with broadband response," Nanophotonics **1**, 17–22 (2012).
27. H. W. Lee, G. Papadakis, S. P. Burgos, K. Chander, A. Kriesch, R. Pala, U. Peschel, and H. A. Atwater, "Nanoscale conducting oxide PlasMOStor," Nano Lett. **14**, 6463–6468 (2014).
28. A. J. Sabbah and D. M. Riffe, "Femtosecond pump-probe reflectivity study of silicon carrier dynamics," Phys. Rev. B **66**, 165217 (2002).
29. V. Van, T. A. Ibrahim, K. Ritter, P. P. Absil, F. G. Johnson, R. Grover, J. Goldhar, and P. T. Ho, "All-optical nonlinear switching in GaAs-AlGaAs microring resonators," IEEE Photon. Technol. Lett. **14**, 74–76 (2002).
30. D. A. Neamen, *Semiconductor Physics and Devices Basic Principles* (McGraw-Hill, 2003).
31. E. S. Harmon, M. R. Melloch, J. M. Woodall, D. D. Nolte, N. Otsuka, and C. L. Chang, "Carrier lifetime versus anneal in low temperature growth GaAs," Appl. Phys. Lett. **63**, 2248–2250 (1993).
32. N. P. Wells, P. M. Belden, J. R. Demers, and W. T. Lotshaw, "Transient reflectivity as a probe of ultrafast carrier dynamics in semiconductors: a revised model for low-temperature grown GaAs," J. Opt. A Pure Appl. Opt. **116**, 073506 (2014).
33. S. Gupta, M. Y. Frankel, J. A. Valdmanis, J. F. Whitaker, G. A. Mourou, F. W. Smith, and A. R. Calawa, "Subpicosecond carrier lifetime in GaAs grown by molecular beam epitaxy at low temperatures," Appl. Phys. Lett. **59**, 3276–3278 (1991).
34. S. Gupta, J. F. Whitaker, and G. A. Mourou, "Ultrafast carrier dynamics in III-V semiconductors grown by molecular-beam epitaxy at very low substrate temperatures," IEEE J. Quantum Electron. **28**, 2464–2472 (1992).
35. L. Nevou, J. Mangeney, M. Tchernycheva, F. H. Julien, F. Guillot, and E. Monroy, "Ultrafast relaxation and optical saturation of intraband absorption of GaN/AlN quantum dots," Appl. Phys. Lett. **94**, 132104 (2009).
36. N. Iizuka, K. Kaneko, and N. Suzuki, "Near-infrared intersubband absorption in GaN/AlN quantum wells grown by molecular beam epitaxy," Appl. Phys. Lett. **81**, 1803–1805 (2002).
37. N. Iizuka, K. Kaneko, and N. Suzuki, "All-optical switch utilizing intersubband transition in GaN quantum wells," IEEE J. Quantum Electron. **42**, 765–771 (2006).
38. V. Ortiz, J. Nagle, and A. Alexandrou, "Influence of the hole population on the transient reflectivity signal of annealed low-temperature-grown GaAs," Appl. Phys. Lett. **80**, 2505–2509 (2002).
39. C. H. Lee, A. Antonetti, and G. Mourou, "Measurements on the photoconductive lifetime of carriers in GaAs by optoelectronic gating technique," Opt. Commun. **21**, 158–161 (1977).
40. K. F. Lamprecht, S. Juen, L. Palmetshofer, and R. A. Hopfel, "Ultrashort carrier lifetimes in H+ bombarded InP," Appl. Phys. Lett. **59**, 926–928 (1991).
41. F. E. Doany, D. Grischkowsky, and C. C. Chi, "Carrier lifetime versus ion-implantation dose in silicon on sapphire," Appl. Phys. Lett. **50**, 460–462 (1987).
42. D. H. Auston, P. Lavallard, N. Sol, and D. Kaplan, "An amorphous silicon photodetector for picosecond pulses," Appl. Phys. Lett. **36**, 66–68 (1980).
43. A. Esser, K. Seibert, H. Kurz, G. N. Parsons, C. Wang, B. N. Davidson, G. Lucovsky, and R. J. Nemanich, "Ultrafast recombination and trapping in amorphous silicon," Phys. Rev. B **41**, 2879–2884 (1990).
44. A. M. Mahmoud and N. Engheta, "Wave-matter interactions in epsilon-and-mu-near-zero structures," Nat. Commun. **5**, 5638 (2014).
45. D. Traviss, R. Bruck, B. Mills, M. Abb, and O. L. Muskens, "Ultrafast plasmonics using transparent conductive oxide hybrids in the epsilon-near-zero regime," Appl. Phys. Lett. **102**, 121112 (2013).
46. M. G. Silveirinha and N. Engheta, "Theory of supercoupling, squeezing wave energy, and field confinement in narrow channels and tight bends using ε near-zero metamaterials," Phys. Rev. B **76**, 245109 (2007).
47. G. Naik and A. Boltasseva, "Plasmonics and metamaterials: looking beyond gold and silver," SPIE Newsroom (30 January 2012), doi: 10.1117/2.1201201.004077.
48. A. V. Singh, R. M. Mehra, N. Buthrath, A. Wakahara, and A. Yoshida, "Highly conductive and transparent aluminum-doped zinc oxide thin films prepared by pulsed laser deposition in oxygen ambient," J. Opt. A Pure Appl. Opt. **90**, 5661–5665 (2001).

49. H. Kim, J. S. Horwitz, S. B. Qadri, and D. B. Chrisey, "Epitaxial growth of Al-doped ZnO thin films grown by pulsed laser deposition," Thin Solid Films **420**, 107–111 (2002).
50. D. Ashkenasi, M. Lorenz, and A. Rosenfeld, "Surface damage threshold and structuring of dielectrics using femtosecond laser pulses: the role of incubation," Appl. Surf. Sci. **150**, 101–106 (1999).
51. R. Boyd, *Nonlinear Optics* (Elsevier, 2008).
52. A. Janotti and C. G. V. de Walle, "Oxygen vacancies in ZnO," Appl. Phys. Lett. **87**, 122102 (2005).
53. J. Kim, G. V. Naik, A. V. Gavrilenko, K. Dondapati, V. I. Gavrilenko, S. M. Prokes, O. J. Glembocki, V. M. Shalaev, and A. Boltasseva, "Optical properties of gallium-doped zinc oxide—a low-loss plasmonic material: first-principles theory and experiment," Phys. Rev. X **3**, 041037 (2013).
54. L. Alloatti, R. Palmer, S. Diebold, K. P. Pahl, B. Chen, R. Dinu, M. Fournier, J. M. Fedeli, T. Zwick, W. Freude, C. Koos, and J. Leuthold, "100 GHz silicon-organic hybrid modulator," Light Sci. Appl. **3**, e173–e177 (2014).
55. M. R. Watts, W. A. Zortman, D. C. Trotter, R. W. Young, and A. L. Lentine, "Vertical junction silicon microdisk modulators and switches," Opt. Express **19**, 21989–22003 (2011).
56. E. Timurdogan, C. M. Sorace-Agaskar, J. Sun, E. S. Hosseini, A. Biberman, and M. R. Watts, "An ultralow power athermal silicon modulator," Nat. Commun. **5**, 4008 (2014).
57. Q. Xu, S. Manipatruni, B. Schmidt, J. Shakya, and M. Lipson, "12.5 Gbit/s carrier-injection-based silicon micro-ring silicon modulators," Opt. Express **15**, 430–436 (2007).